Applied Catalysis B: Environmental 256 (2019) 117877

Contents lists available at ScienceDirect

Applied Catalysis B: Environmental

journal homepage: www.elsevier.com/locate/apcatb

Ternary photocatalyst of atomic-scale Pt coupled with MoS_2 co-loaded on TiO_2 surface for highly efficient degradation of gaseous toluene

Jiafu Qu, Dongyun Chen*, Najun Li, Qingfeng Xu, Hua Li, Jinghui He, Jianmei Lu*

College of Chemistry, Chemical Engineering and Materials Science, Collaborative Innovation Center of Suzhou Nano Science and Technology, Soochow University, Suzhou, 215123, China

ARTICLE INFO

Keywords:
TiO_2 nanosheets
Molybdenum disulfide
Atomic-scale Pt
Photocatalytic oxidation
Toluene removal

ABSTRACT

Photocatalysis by semiconducting materials loaded with non-metal or noble metals is an excellent strategy for removal of gaseous toluene. Herein, a new photocatalytic system was successfully prepared *via* simultaneously coupling atomic-scale Pt with MoS_2 as co-catalysts to load on the surface of TiO_2. The obtained photocatalysts exhibited good performance in toluene degradation by promoting the separation of photogenerated electron-hole pairs. The most efficient toluene degradation was achieved by the photocatalyst with a content of 2.0 wt% Pt-MT-1.0 (i.e., coupling 2.0 wt% atomic-scale Pt with 1.0 wt% MoS_2), with a conversion ratio of 91.5%. This conversion ratio was higher than those of platinum-free MT-1.0 (33.9%) and pure TiO_2 (72.3%). The results demonstrate the potential application of this new nanocomposite for efficient photocatalytic degradation of toluene.

1. Introduction

Toluene is one of the most common indoor volatile organic compounds (VOCs), emitted from construction/decorative materials, furniture, and oil paints [1–3]. Toluene exposure can lead to various health disorders, such as memory impairment, headache, or nausea [4–6]. Because people in modern societies spend about 90% of their time indoors, effective remediation of toluene pollution is necessary for human health [6,7]. Various disposal methods have been applied to treat toluene pollution, such as adsorption, catalytic combustion, bioreaction, and heterogeneous photocatalytic oxidation [8–11]. Among these, the most attractive is heterogeneous photocatalytic oxidation, because of its efficiency, cost-effectiveness, and mild operating conditions.

Various photocatalysts have been used for toluene treatment, such as TiO_2, C_3N_4, Ta_2O_5, WO_3, and $ZnFe_2O_4$ [12–16]. Among these candidates, TiO_2 has received significant attention for its stability, non-toxicity, availability, relatively low cost, and high activity [17,18]. However, the application of TiO_2 is limited by the tendency to undergo recombination of charge carriers and its inability to be activated by visible light. To overcome these issues, numerous methods have been used for enhancing the photocatalytic performance of TiO_2, such as modifying the TiO_2 surface, hybridization with metals or non-metals, and compositing with other semiconductors [19–22]. Notably, the photocatalytic activity of TiO_2 can be significantly enhanced by coupling with non-metals or metals as co-catalysts.

Recently, two-dimensional (2D) MoS_2 materials have attracted wide attention because of their unique physical and chemical properties [23–26]. MoS_2 materials possess numerous exposed edges, with the exposed sulfur atoms behaving as active sites, which promote their photocatalytic and electrocatalytic performance [27–29]. In addition, MoS_2 is a good candidate as a support material for isolated metal atoms because of its unique structure. For example, Yuan and coworkers reported a simple method to synthesize a 2D-2D MoS_2/TiO_2 photocatalyst that possessed high activity for solar hydrogen generation [18]. Shi and coworkers prepared Zn-doped MoS_2 catalysts that exhibited excellent electrocatalytic activity for the hydrogen evolution reaction because of their increased density of active sites and optimized three-dimensional (3D) electron configuration [30]. Therefore, the use of MoS_2 as a co-catalyst for toluene degradation is an interesting prospect.

Moreover, surface modification of photocatalysts through introduction of noble metals, such as Pt, Au, and Ag, is also an attractive method to enhance the photocatalytic activity [31–33]. Recently, single-atom metals have been attracting considerable attention because they maximize the atomic efficiency [34–36]. Fang et al. confined single Pt atoms into a metal–organic framework for efficemient photocatalytic H_2 production [37]. Likewise, Li et al. anchored isolated Pt atoms on g-C_3N_4 for enhancing the photocatalytic H_2 evolution activity [38]. Therefore, Pt may be an ideal co-catalyst in photocatalytic toluene degradation.

* Corresponding authors.
E-mail addresses: dychen@suda.edu.cn (D. Chen), lujm@suda.edu.cn (J. Lu).

https://doi.org/10.1016/j.apcatb.2019.117877
Received 16 March 2019; Received in revised form 14 June 2019; Accepted 17 June 2019
Available online 19 June 2019
0926-3373/

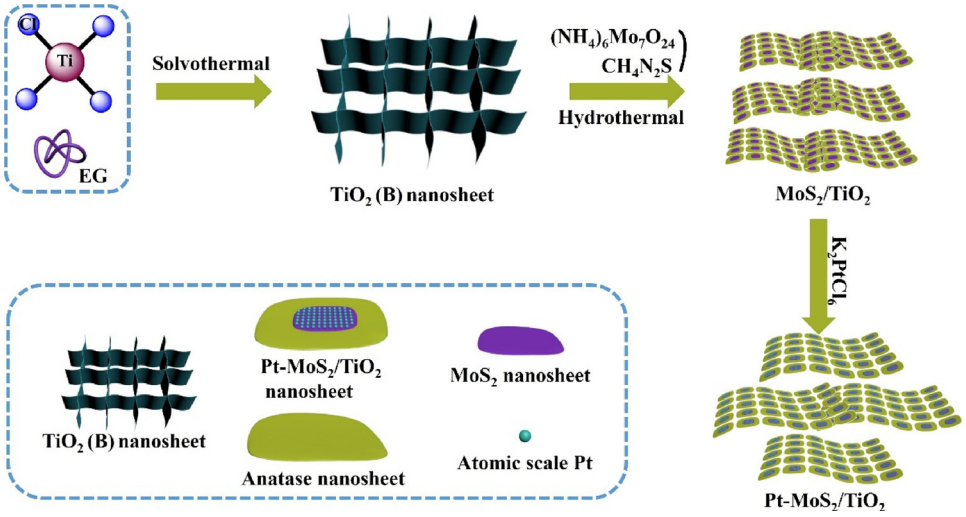

Scheme 1. Illustration of the fabrication of Pt-MoS_2/TiO_2.

Many studies have reported the photocatalytic degradation of toluene by introduction of either non-metals or single-atom metals as co-catalysts. However, the strategy of improving the photocatalytic performance by simultaneous coupling with non-metals and single-atom metals as co-catalysts has been less well explored. Herein, we demonstrate that atomic-scale Pt and MoS_2, as a new combination of co-catalysts loaded on the TiO_2 surface, can remarkably enhance the photocatalytic performance for toluene degradation. First, the MoS_2/TiO_2 composites were formed by a facile hydrothermal reaction, and then the Pt-MoS_2/TiO_2 composites were fabricated by a stirring method at room temperature (Scheme 1). The structure, composition, and photocatalytic activity of a series of such catalysts were investigated. The toluene conversion reached 91.5% after 25 min, an improvement of catalytic efficiency by 58.6% compared with MoS_2/TiO_2.

2. Experimental section

2.1. Materials

All chemicals were used as received without further purification. Titanium tetrachloride ($TiCl_4$), ethylene glycol (EG), hexaammonium heptamolybdate tetrahydrate and thiourea were of analytic grade and purchased from the Sinopharm Chemical Reagents Co., Ltd. Potassium hexachloroplatinate(iv) (K_2PtCl_6, > 99.9%) was purchased from Sigma-Aldrich.

2.2. Instrumentation

The morphology and microstructures in the fabrication process of Pt-MoS_2/TiO_2 (Pt-MT) were observed by using transmission electron microscope (TEM) (FEI Tecnai G-20) with 200 kV acceleration voltage, scanning electron microscopy (SEM) (Hitachi S-4700), high angle annular dark field scanning transmission electron microscopy (HAADF-STEM) (FEI Tecnai F-20). X-ray diffraction (XRD; X' Pert-Pro MPD) and high-resolution TEM (HRTEM) were used to analyze the crystal phase. The diffuse reflectance infrared Fourier transform (DRIFT) spectroscopy were analysed the CO adsorption behavior. The composition of Pt-MT and the percentage of Pt in catalysts were analysed by X-ray photoelectron spectroscopy (XPS) (ESCALAB 250Xi) and inductively coupled plasma (ICP) (ICAPTM Qc), respectively. UV–vis spectrophotometer (Shimadzu UV-3600) were used to record the UV–vis diffuse reflectance spectra (UV–vis DRS) of samples. And using the fluorescence spectrophotometer (FLS920) to measure the photoluminescence (PL) spectra with an excitation wavelength of 250 nm. The photocurrent and electrochemical impedance spectroscopy (EIS) were characterized by using the electrochemical workstation with CHI 660B electrochemical system (Shanghai, China). The convention of toluene was analyzed by GCMS-QP2020.

2.3. Preparation of TiO_2 (B)

The TiO_2 (B) material was synthesized according to a modified synthetic method. In a typical synthesis of TiO_2 (B), 5 ml of $TiCl_4$ was dissolved in 150 mL EG to form a homogenous solution at room temperature. Then 5 mL ultra-pure water was added to this solution under stirring. Subsequently, the homogeneous light yellow mixture solution was transferred to a stainless-steel autoclave, then, heated at 150 °C for 4 h. The products were obtained by centrifugation, and washed with water and ethanol several times. Whereafter, the white solid were dried at vacuum oven.

2.4. Preparation of MoS_2/TiO_2

The 2D-2D MoS_2/TiO_2 composite photocatalysts were prepared by hydrothermal reactions of the TiO_2 (B) obtained above in an aqueous solution with hexaammonium heptamolybdate tetrahydrate and thiourea. Typically, to a dispersion of TiO_2 (B) (200 mg) in 70 mL ultra-pure water consisting of 2.2 mg hexaammonium heptamolybdate tetrahydrate and 1.9 mg thiourea. Then the mixture was transferred to a stainless-steel autoclave, heated at 220 °C for 18 h. After the reaction, the products were separated out, washed with ethanol and water several times. The formed sample was dried at vacuum oven to give a 1.0 wt% MoS_2/TiO_2 (noted as MT-1.0). In addition, the other catalysts with different mass ratio of MoS_2 and TiO_2 were also fabricated by changing the amount of hexaammonium heptamolybdate tetrahydrate and thiourea. Pristine MoS_2 nanosheets were synthesized by the same strategy but without TiO_2 (detailed in supporting information).

2.5. Preparation of Pt-MoS_2/TiO_2

In a typical synthesis of 2.0 wt% Pt-MT-1.0, 200 mg of MoS_2/TiO_2 nanosheets were dispersed in 15 ml of deionized water and 35 ml of ethanol in a 150 ml flask under stirring for 10 min. Afterward, 30 ml of K_2PtCl_6 (0.15 mM) was added into the flask through a syringe pump at a rate of 10 $ml{\cdot}h^{-1}$ under stirring at room temperature. The solution was stirred for another 1 h after the completion of the addition of K_2PtCl_6 solution. Finally, the sample was collected, washed with ethanol and water for several times, and dried at 60 °C under vacuum.

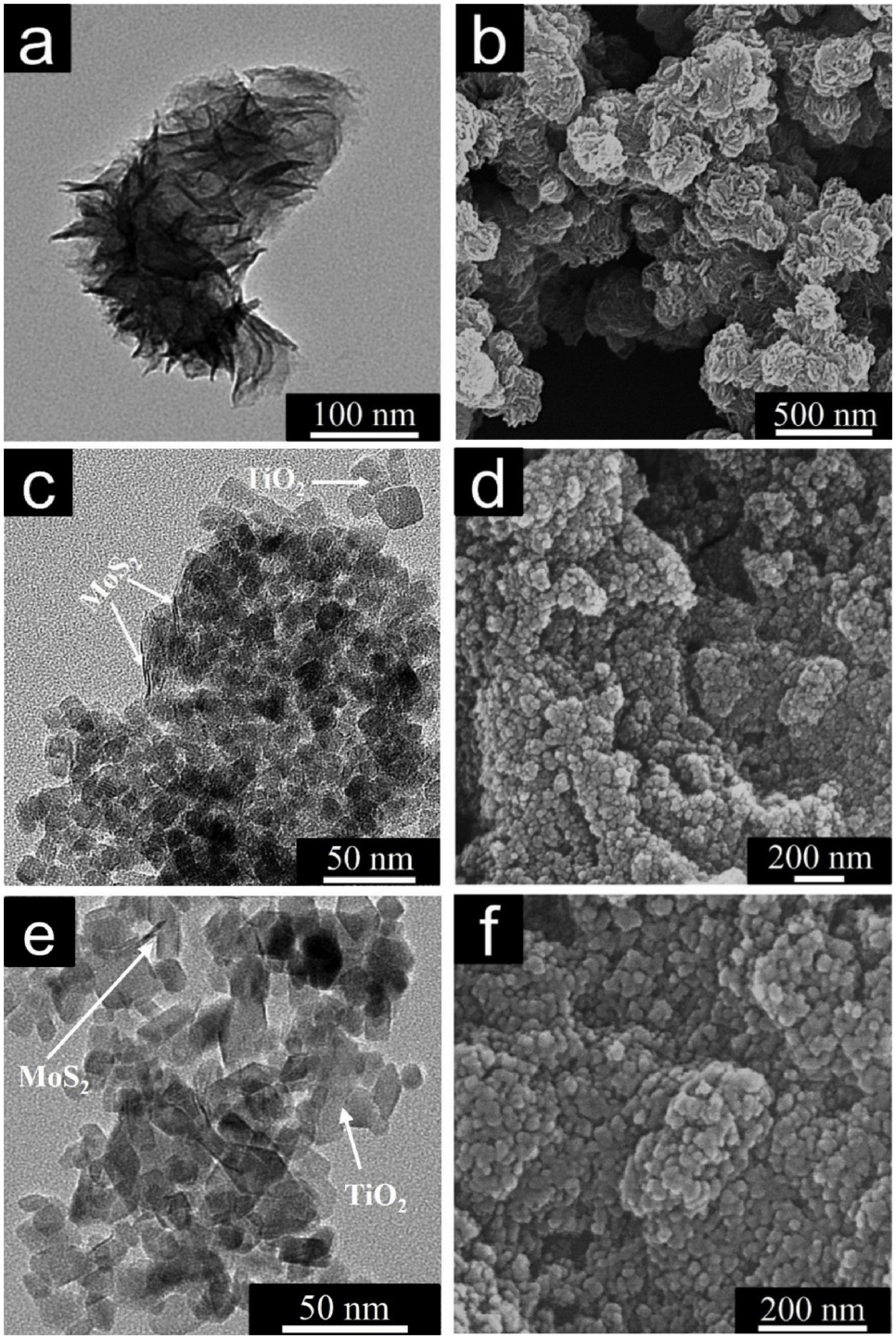

Fig. 1. TEM (a) and SEM (b) images of TiO_2 (B); TEM (c) and SEM (d) images of MT-1.0; TEM (e) and SEM (f) images 2.0 wt% Pt- MT-1.0.

2.6. Photocatalytic oxidation of toluene

A fixed-bed reactor system using 50 mg catalyst at atmospheric pressure was used to photocatalytic oxidation of toluene. A 300 W Xenon lamp (simulated solar light) was fixed vertically 10 cm above the reactor. And the 50 mg catalyst was sprayed on the ITO glass (8 mm width*150 mm length) and putted into the reactor. Then, the mixed gas (50 ppm toluene, balanced in air) were introduced. And the humidity was controlled by bubbling the mixed gas through a glass bottle that contained deionized water. The total gas flow rate was 25 mL min^{-1} and the weight hourly space velocity of total gaseous reactant was 30,000 mL h^{-1} g^{-1}, and the concentrations of toluene were analyzed by GCMS (QP2020).

3. Results and discussion

The structure and morphology of TiO_2 (B) and 2 wt% Pt-MT-1.0 were characterized by TEM and SEM. Fig. 1a shows a TEM image of the TiO_2 (B) nanosheets, which possessed lengths of several hundreds of nanometers. The structure of the nanosheets was also ultra-thin, with some folding observable in the TEM image. The morphology of TiO_2 (B) was further observed by SEM, which likewise demonstrated that the

Table 1
The Pt and Mo contents of catalysts measured by ICP-AES.

Catalysts	Pt contents		Mo contents	
	Theoretical	Actual	Theoretical	Actual
Pt-MT-1.0	0.25 wt%	0.08 wt%	0.5 wt%	0.41 wt%
Pt-MT-1.0	0.5 wt%	0.21 wt%	1.0 wt%	0.89 wt%
Pt-MT-1.0	1.0 wt%	0.32 wt%	2.0 wt%	1.76 wt%
Pt-MT-1.0	2.0 wt%	0.45 wt%	3.0 wt%	2.45 wt%

product consisted of sheet-shaped structures. The MT-1.0 catalysts were then synthesized by a facile hydrothermal reaction. As shown in Fig. 1c, the TiO_2 (B) nanosheets were broken down into numerous small nanoplates after hydrothermal treatment, and each nanoplate was ~12 nm in length. Interestingly, the phase of the small nanoplates was anatase TiO_2 rather than TiO_2 (B), according to analysis by powder XRD. This phase transition was caused by the instability of TiO_2 (B) under high temperature and pressure. The structure of the anatase TiO_2 nanoplates was also characterized by SEM (Fig. 1d), which showed that they possessed a flaky morphology. The TEM and SEM images in Fig. 1e, f indicate that 2.0 wt% Pt was loaded on the surface of MT-1.0 after fabrication of 2 wt% Pt-MT-1.0. According to a previous report by Zeng et al., Pt atoms intercalated into MoS_2 will occupy the positions of Mo atoms [39]. In addition, no formation of Pt nanoparticles was observed in the TEM image. Accordingly, the Pt atoms in the catalysts may be considered to be atomically dispersed. These conclusions were also confirmed by the diffuse reflectance infrared Fourier transform spectroscopy (DRIFTS) and XPS spectra. Furthermore, the Pt and Mo content of the as-prepared samples was measured by inductively coupled plasma–atomic emission spectrometry (ICP-AES) and is listed in Table 1. The actual Pt content of the 2.0 wt% Pt-MT-1.0 catalyst was found to be 0.45 wt%, and the actual content of Mo in the different catalysts are 0.41, 0.89, 1.76 and 2.45 wt%, respectively.

The elemental composition and distributions of Pt, Ti, O, Mo, and S were confirmed by HAADF-STEM imaging and the corresponding EDX mappings. A representative HAADF-STEM image is shown in Fig. 2a, in which no Pt atoms can be observed because of their low content and good atomic dispersion. The corresponding STEM-EDX and TEM-EDX mapping images are shown in Fig. 2c-f and Figure S1, the mapping image (Figure S1) showed that the major population of Pt were distributed on MoS_2, and the images of Ti, O, Mo, and S indicated that Ti and O were distributed uniformly, and that MoS_2 was successfully loaded on the surface of TiO_2. It is apparent from the images that nanojunctions were formed between MoS_2 and TiO_2. In addition, the EDX spectra of different region were also investigated in Figure S2, demonstrating the uniform distribution of Ti, O, Mo, S and Pt element. Further confirmation of the formation of nanojunctions was obtained from the HRTEM image in Fig. 2b. Two interplanar lattice spacings of 0.60 and 0.35 nm are clearly discernible, corresponding to the (002) crystallographic planes of MoS_2 and (101) crystal facet of anatase TiO_2, respectively. It is worth noting that nanojunctions contribute to the separation of photogenerated charge and hole pairs, which are a primary factor in promoting the photocatalytic activities of the photocatalysts in toluene oxidation. In addition, the loading of atomic Pt in catalysts tends to further promote the transfer of photogenerated charge carriers, improving the photocatalytic activities.

The XRD patterns of TiO_2 (B), MoS_2, and 2D-2D MoS_2/TiO_2 catalysts with different MoS_2 mass ratios are displayed in Fig. 3a. For pure TiO_2 (B), all diffraction peaks were consistent with the standard values (JCPDS 074–1940), demonstrating that the TiO_2 (B) was successfully synthesized [40]. For pure MoS_2, the three main peaks at $2\theta = 14.06^\circ$, 33.27°, and 57.45° were attributed to the (002), (100), and (106) planes, respectively. After the hydrothermal reactions, the diffraction peaks of TiO_2 significantly changed, indicating a phase transition of the unstable TiO_2 (B). The new diffraction peaks at $2\theta = 25.44^\circ$, 38.20°, 48.29°, 54.22°, 55.30°, 62.82°, 70.48°, 75.58°, and 76.52° were ascribed to the (101), (004), (200), (105), (211), (204), (220), (215), and (301) reflections of anatase TiO_2, respectively [18]. There were no peaks of MoS_2 in the patterns, confirming the low content of MoS_2. In addition, the XRD patterns of MT-1.0 with different atomic Pt loading are also

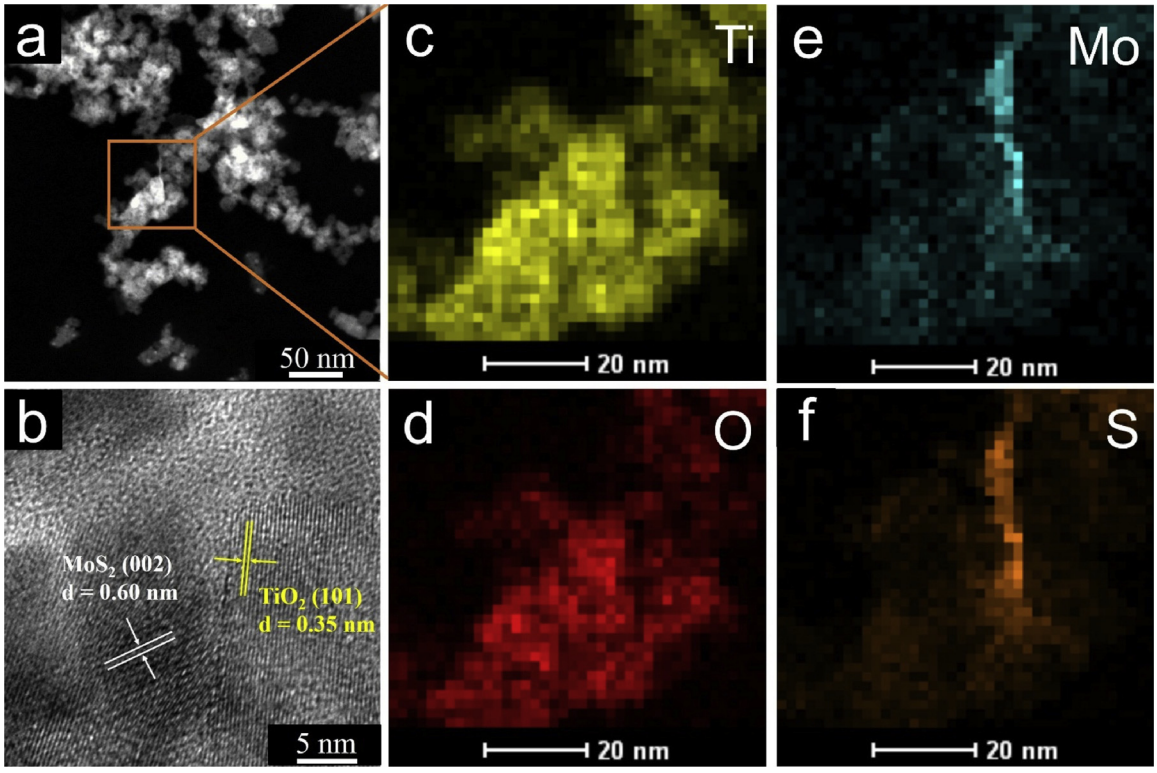

Fig. 2. The HAADF-STEM (a), HRTEM (b) images and STEM EDX mappings (c–f) of 2.0 wt% Pt-MT-1.0.

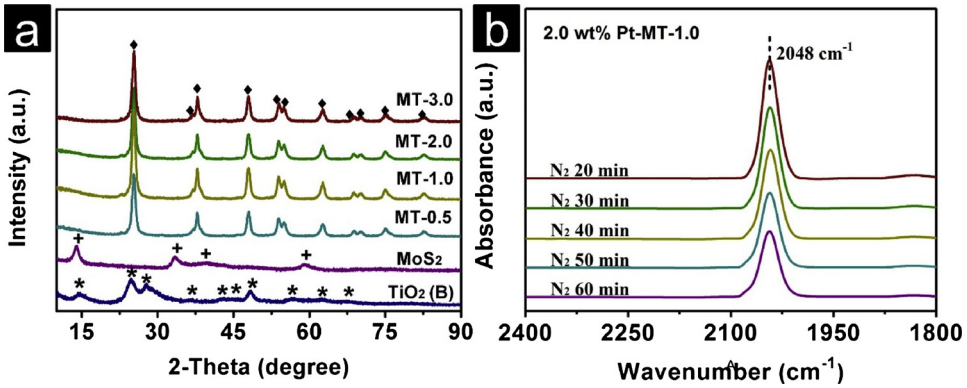

Fig. 3. (a) XRD patterns of TiO_2 (B), MoS_2, and MoS_2/TiO_2 samples with different MoS_2 contents. '◆', '+', and '*' refer to the crystalline phase of TiO_2 (anatase), MoS_2, and TiO_2 (B), respectively. (b) DRIFTS spectra of CO adsorption for 2.0 wt% Pt-MT-1.0 after being purged with N_2 gas for different lengths of time.

presented in Figure S3. As can be seen, there were no differences between the patterns of pure MT-1.0 and MT-1.0 with different Pt loading.

The CO adsorption behavior of 2.0 wt% Pt-MT-1.0 was measured by DRIFTS (Fig. 3b). As can be clearly seen, only one peak was found, at 2048 cm^{-1}, which showed the atomically dispersion of Pt on the support [41,48]. No peaks corresponding to bridge-adsorbed CO in the range 1920-1950 cm^{-1} were observed. This further confirmed that the Pt atoms in the catalysts were atomically dispersed. In addition, we also measured the CO adsorption behavior of 2.0 wt% Pt-MT-1.0 after CO saturation and at 1, 5 and 10 min under a N_2 flow (Figure S4a). It can be seen that the catalyst has a well CO adsorption strength. And the CO adsorption behavior at different temperature was also tested (Figure S4b), there is a negatively shift due to the influence of temperature. The presence of atomic Pt-modified MoS_2 on TiO_2 was further confirmed by the XPS spectra (Fig. 4a), which contained the expected Ti, O, Mo, S, and Pt peaks. Fig. 4b shows the Ti 2p spectrum, with two main signals characteristic of the Ti $2p_{3/2}$ and Ti $2p_{1/2}$ levels, with binding energies of 458.6 and 464.4 eV, respectively. Additionally, the high-resolution XPS spectrum of Mo 3d for 2.0 wt% Pt-MT-1.0 is shown in Fig. 4c. These reveal an interesting finding. There is an obvious difference between the Mo 3d peaks of 2.0 wt% Pt-MT-1.0 and those of MT-1.0 (Figure S5), in which a shift of about 0.5 eV occurs after the introduction of atomic Pt, suggesting that the atomic Pt doping increased the electronic density in MoS_2 [25]. In addition, the Pt 4f spectra showed two main peaks at 72.7 eV and 76.0 eV (Fig. 4d). The lower of these is remarkably positively shifted (by 1.5 eV) relative to the corresponding peak of Pt foil (71.2 eV), providing further evidence that the Pt atoms were atomically dispersed in the catalysts [25,42].

The UV–vis DRS spectra were recorded and converted to absorption spectra to study the optical properties of the various samples (Fig. 5). As shown in Fig. 5a, pure TiO_2 exhibited a photoabsorption edge at the ultraviolet region (shorter than 400 nm). After MoS_2 loading on TiO_2, the MoS_2/TiO_2 composites showed absorption bands at wavelengths larger than 400 nm, verifying that the composites showed increased absorption of visible light compared with TiO_2. In addition, with the increasing content of MoS_2, the absorption intensity increased

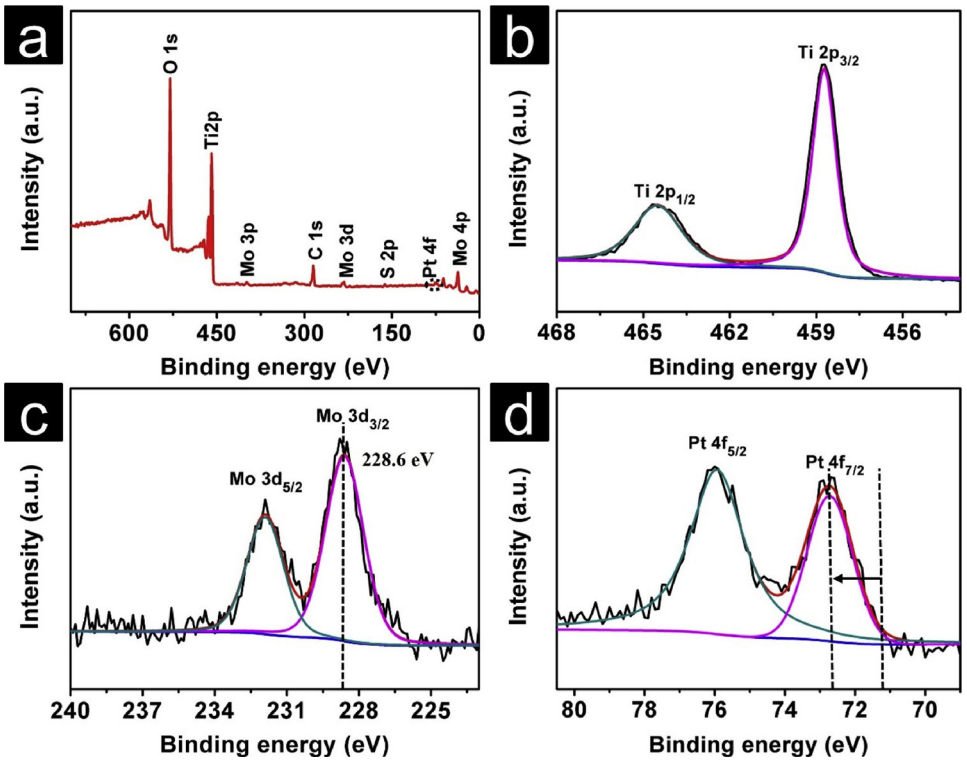

Fig. 4. XPS survey spectra of 2.0 wt% Pt-MT-1.0 (a); high-resolution XPS spectrum of the Ti 2p (b), Mo 3d (c), and Pt 4f (d) regions.

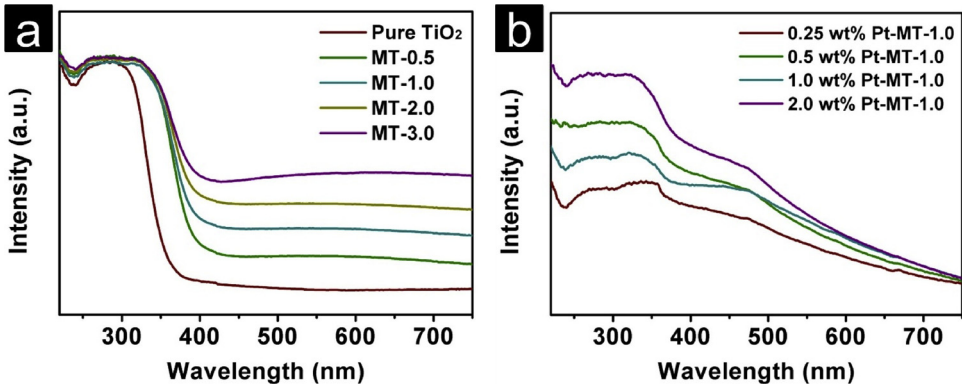

Fig. 5. (a) UV–vis DRS analysis of TiO_2 with different amounts of MoS_2; (b) UV–vis DRS analysis of MT-1.0 with different amounts of Pt.

gradually, which is consistent with the observed color change from the initial white to gray. Fig. 5b shows the UV–vis spectra of MT-1.0 with different amounts of Pt. It is clear that the absorption thresholds gradually increases with the addition of atomic Pt supported on the catalyst. In other words, the electronic structure of the catalyst is significantly modified by the introduction of the atomic Pt. This might be attributed to the interaction between Pt and MT, which is consistent with the results of above XPS. Furthermore, the PL spectra of TiO_2, MT-1.0, and 2.0 wt% Pt-MT-1.0 were also recorded, as given in Figure S6. It is clear that the latter two exhibit a lower emission intensity than that of pure TiO_2, presumably as a result of heterojunction formation and the introduction of atomic Pt, indicating the suppressed recombination of photogenerated electrons in MT-1.0 and 2.0 wt% Pt-MT-1.0.

To further evaluate the recombination efficiency of the photogenerated electrons, the photocurrent and electrochemical impedance spectroscopy (EIS) responses of the various samples were measured. Fig. 6a shows the photocurrent response of MoS_2/TiO_2 composites with different MoS_2 contents under irradiation of a 300 W Xe lamp and four periodic on/off cycles. It was observed that the photocurrent response of the MoS_2/TiO_2 composites was higher than that of pure TiO_2. This phenomenon was caused by the MoS_2 loading on the surface of the TiO_2 nanosheets, which efficiently suppressed the rapid recombination of photogenerated electron–hole pairs. The transient photocurrents of MT-1.0 loaded with different amounts of Pt were also investigated (Fig. 6c), in which the transient photocurrent increased gradually with increasing Pt content, indicating that the introduction of atomic Pt further suppressed the recombination of photogenerated electron-hole pairs. Moreover, the EIS spectra of all samples were also recorded under the same conditions (Fig. 6b, d). The MT-1.0 and 2.0 wt% Pt-MT-1.0 samples showed the smallest arc radii, which is consistent with the above conclusion regarding suppressed electron–hole recombination.

The photocatalytic activities of the as-prepared catalysts were investigated through their ability to remove gaseous toluene (50 ppm) in an air atmosphere under the irradiation of a Xe lamp. As shown in Fig. 7a, the pure TiO_2 achieved a poor photocatalytic performance with a gaseous toluene conversion of only 19.2%, which can be attributed to the rapid recombination of photogenerated carriers. However, the MoS_2/TiO_2 composites clearly photo-catalyzed the degradation of toluene with a higher efficiency, which can be attributed to the synergistic interaction between the two component materials. Interestingly, the photocatalytic efficiency for degradation of toluene was maximized after loading of only 1.0 wt% MoS_2, removing 57.6% of toluene at 25 min. Although the toluene conversion increased significantly when raising the content of MoS_2 from zero to 1.0 wt%, it

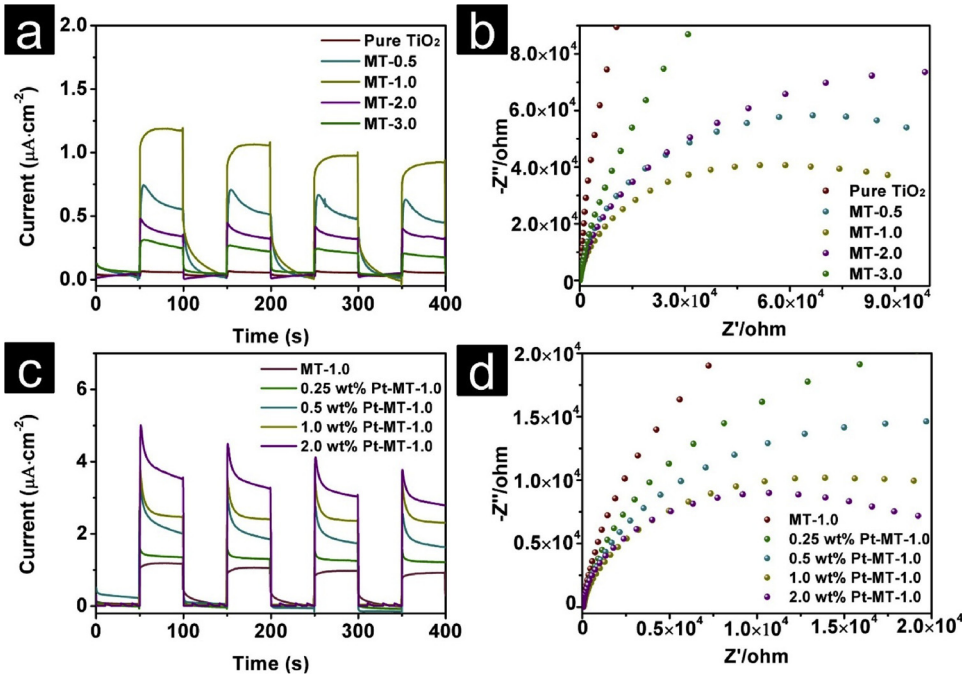

Fig. 6. (a), (c) Transient photocurrent and (b), (d) electrochemical impedance spectra of the samples.

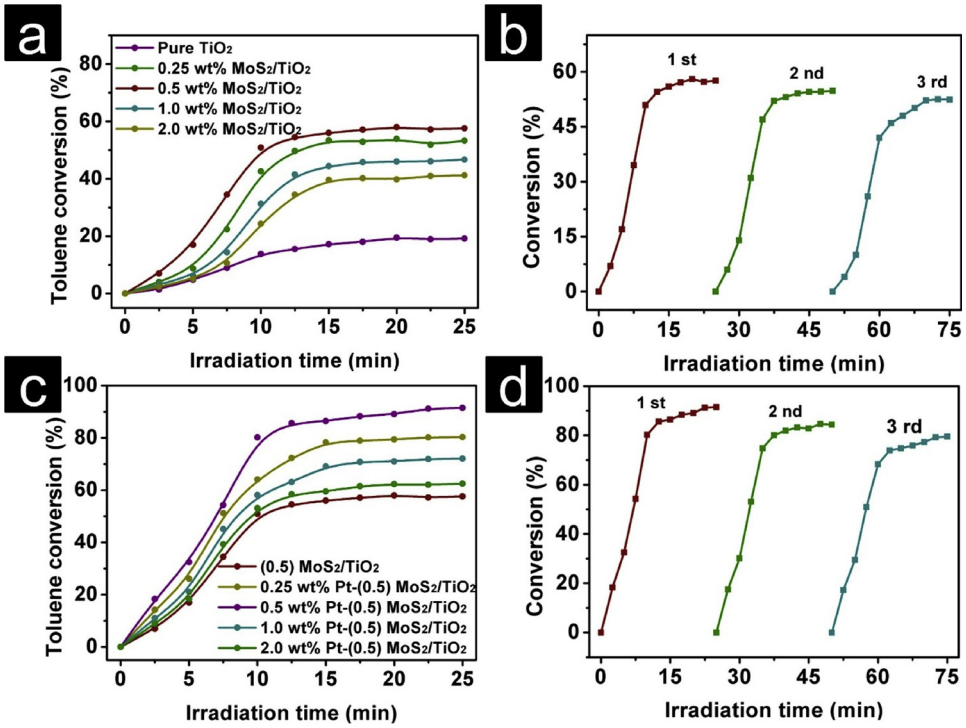

Fig. 7. (a), (c) Visible-light photocatalytic activities of the as-prepared samples for toluene removal in air (50 ppm); (b), (d) the durability of the catalyst for toluene oxidation.

began to decrease after this point. The most likely reason for this phenomenon is the shading effect, in which the absorption of the incident light by the TiO_2 component is prevented by MoS_2. Fig. 7b shows the results of the durability testing of MT-1.0. The efficiency of toluene degradation decreased slightly after 3 cycles, demonstrating its good stability for toluene oxidation. In addition, to investigate the influence of atomic Pt in the system, the photocatalytic activity of MT-1.0 with different atomic Pt loading was measured and is displayed in Fig. 7c. It is clear that the photocatalytic activity continually increased with increasing Pt content. The results also indicated that the MoS_2 and atomic Pt components play an important simultaneous role in the photocatalytic system. The 2.0 wt% Pt-MT-1.0 catalyst showed the optimal performance, with an extremely high photocatalytic activity of 91.5% after 25 min, demonstrating that the simultaneous presence of MoS_2 and atomic Pt more effectively inhibited the recombination of photogenerated electron–hole pairs. The reaction rate (r) of toluene over 2.0 wt% Pt-MT-1.0 was calculated as 8.9×10^{-8} mol·s^{-1} g^{-1}. In addition, the true and apparent quantum efficiency of the catalyst (50 mg) were also calculated as 0.46 % and 0.2 % according to the reported reference [13,43,44]. The 2.0 wt% Pt-MT-1.0 catalyst was also used in a durability test (Fig. 7d); after 3 cycles, it retained good photocatalytic activity for toluene oxidation. In addition, the performance of 2.0 wt% Pt-MT-1.0 is compared with several previously reported photocatalysts for degradation of toluene in Table 2. As can be seen, 2.0 wt% Pt-MT-1.0 showed better performance for toluene oxidation.

The reaction mechanism for the photocatalytic toluene degradation is displayed in Scheme 2. The band energy (Eg) and valence band (VB)

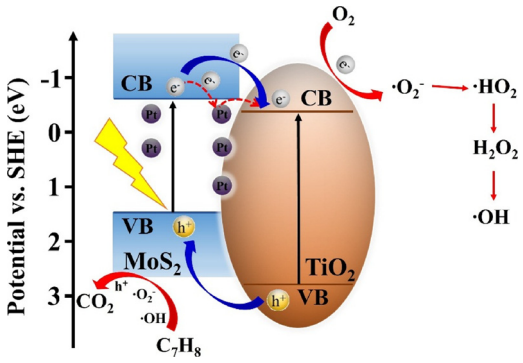

Scheme 2. Photocatalytic mechanism of toluene removal.

maximum (measured by XPS) of TiO_2 were 3.2 eV and 2.8 eV, respectively (Figure S7). Considering these values in the light of previous mechanistic studies, we propose the following pathways for the degradation process [4,47]. Firstly, the 2.0 wt% Pt-MT-1.0 generated electron-hole pairs under the irradiation of the Xe lamp. The produced electrons and holes then participated in a sequence of reactions to form various oxygen-containing radicals. Finally, the hydroxy radicals generated on the TiO_2 surface oxidized toluene to CO_2. The reactions involved in this mechanism of photocatalytic oxidation of toluene are as follows.

$$Pt - MT + hv \rightarrow e^- + h^+ \quad (1)$$

Table 2
Comparison of toluene degradation time and conversion for 2.0 wt% Pt-MT-1.0 with previously reported catalysts for toluene removal.

Photocatalysts	Light source	Toluene concentration (ppm)	Degradation time (min)	Conversion (%)	Ref.
2.0 wt% Pt-MT-1.0 (50 mg)	300W Xe lamp	50	25	91.5	Our work
0.5% ZnO/P25-500 (200 mg)	300W Xe lamp	500	100	100	[45]
0.7% Fe-TiO_2 (1200 mg)	300W Xe-arc lamp	370	120	96.5	[46]
$TiBi_{1.9\%}Zn_{1\%}O_2$ (100 mg)	300W Xe lamp	280	200	93	[11]

$$OH^-(surface) + h^+ \rightarrow \bullet OH \quad (2)$$

$$O_2 + e^- \rightarrow \bullet O_2^- \quad (3)$$

$$O_2^- + H^+ \rightarrow \bullet HO_2 \quad (4)$$

$$\bullet HO_2 \rightarrow O_2 + H_2O_2 \quad (5)$$

$$H_2O_2 + O_2^- \rightarrow OH^- + \bullet OH + O_2 \quad (6)$$

$$OH\bullet + C_7H_8 \rightarrow C_6H_5CH_2\bullet + H_2O \quad (7)$$

$$C_6H_5CH_2\bullet + O_2 \rightarrow C_6H_5CH_2OO\bullet \rightarrow C_6H_5CHO \rightarrow C_6H_5COOH \quad (8)$$

$$C_6H_5COOH + h^+/\bullet O_2^-/\bullet OH \rightarrow C_6H_6 \rightarrow CO_2 + H_2O \quad (9)$$

4. Conclusions

A unique photocatalytic nanocomposite (Pt-MT) was fabricated to degrade gaseous toluene. This new material exhibited high photocatalytic activity as a result of strong light absorption and superior electron separation capacity. The toluene conversion ratio of 2.0 wt% Pt-MT-1.0 was 91.5%, an enhancement of catalytic efficiency by ˜58.8% compared with the platinum-free MT-1.0 (57.6%), after 25 min. This indicates that the introduction of atomic-scale Pt further facilitates electron separation, and the MoS_2 and atomic-scale Pt components play an important simultaneous role in the photocatalytic system. In addition, the Pt-MT photocatalyst also demonstrates exceptional stability during prolonged toluene oxidation. In summary, Pt-MT shows excellent ability for degradation of toluene and has encouraging potential for the practical remediation of this gaseous pollutant.

Acknowledgements

We gratefully acknowledge the financial support provided by the National Key R&D Program of China (2017YFC0210901, 2017YFC0210906), National Natural Science Foundation of China (51573122, 21722607, 21776190), Natural Science Foundation of the Jiangsu Higher Education Institutions of China (17KJA430014, 17KJA150009) and the project supported by the Priority Academic Program Development of Jiangsu Higher Education Institutions (PAPD).

Appendix A. Supplementary data

Supplementary material related to this article can be found, in the online version, at doi:https://doi.org/10.1016/j.apcatb.2019.117877.

References

[1] C. Abhishek, H. Stefanie, Environ. Sci. Technol. 48 (2014) 14607–14614.
[2] Z. Fan, M. Wang, X. Zhu, B. Hong, W. Wang, Z. Qi, X. Wei, J. Ding, J. Bao, S. Song, Appl. Catal. B-Environ. 170-171 (2015) 215–224.
[3] S. Weon, W. Choi, Environ. Sci. Technol. 50 (2016) 2556–2563.
[4] T.D. Pham, B.K. Lee, J. Hazard. Mater. 300 (2015) 493–503.
[5] S. Weon, J. Choi, T. Park, W. Choi, Appl. Catal. B-Environ. 205 (2017) 386–392.
[6] S. Weon, J. Kim, W. Choi, Appl. Catal. B-Environ. 220 (2018) 1–8.
[7] W.W. Nazaroff, A.H. Goldstein, Indoor Air 25 (2015) 357–361.
[8] M. Kraus, U. Trommler, F. Holzer, F.-D. Kopinke, U. Roland, Chem. Eng. J. 351 (2018) 356–363.
[9] F. Hu, P. Yue, J. Chen, L. Shuai, S. Hua, J. Li, Appl. Catal. B-Environ. 240 (2019) 329–336.
[10] S. Mudliar, B. Giri, K. Padoley, D. Satpute, R. Dixit, P. Bhatt, R. Pandey, A. Juwarkar, A. Vaidya, J. Environ. Manage. 91 (2010) 1039–1054.
[11] J.J. Li, S.C. Cai, Z. Xu, X. Chen, J. Chen, H.P. Jia, J. Chen, J. Hazard. Mater. 325 (2017) 261–270.
[12] J. Ji, Y. Xu, H. Huang, M. He, S. Liu, G. Liu, R. Xie, Q. Feng, Y. Shu, Y. Zhan, Chem. Eng. J. 327 (2017) 490–499.
[13] O. Fontelles-Carceller, M.J. Muã Oz-Batista, N.A.M. Fernã, A. Kubacka, ACS Appl. Mater. Interfaces 8 (2016) 2617–2627.
[14] R. Ullah, H. Sun, H.M. Ang, M.O. Tadé, S. Wang, Ind. Eng. Chem. Res. 52 (2013) 3320–3328.
[15] T. Arai, M. Horiguchi, M. Yanagida, T. Gunji, H. Sugihara, K. Sayama, Chem. Commun. 43 (2008) 5565–5567.
[16] H. Mehrizadeh, A. Niaei, H.H. Tseng, D. Salari, A. Khataee, J. Photochem. Photobiol. A: Chem. 332 (2017) 188–195.
[17] J. Sun, X. Li, J. Ke, D. Zhang, Q. Zhao, J. Phys. Chem. C 118 (2014) 10113–10121.
[18] Y.J. Yuan, Z.J. Ye, H. Lu, B. Hu, Z. Zou, ACS Catal. 6 (2016) 532–541.
[19] M. Nolan, A. Iwaszuk, A.K. Lucid, J.J. Carey, M. Fronzi, Adv. Mater. 28 (2016) 5425–5446.
[20] V. Kumaravel, S. Mathew, J. Bartlett, S.C. Pillai, Appl. Catal. B-Environ. 244 (2019) 1021–1064.
[21] T. Boningari, S.N.R. Inturi, M. Suidan, P.G. Smirniotis, Chem. Eng. J. 339 (2018) 249–258.
[22] W. Tu, Y. Li, L. Kuai, Y. Zhou, Q. Xu, H. Li, X. Wang, M. Xiao, Z. Zou, Nanoscale 9 (2017) 9065–9070.
[23] D. Deng, K.S. Novoselov, Q. Fu, N. Zheng, Z. Tian, X. Bao, Nature Nanotech. 11 (2016) 218–230.
[24] J. Deng, H. Li, J. Xiao, Y. Tu, D. Deng, H. Yang, H. Tian, J. Li, P. Ren, X. Bao, Energy Environ. Sci. 8 (2015) 1594–1601.
[25] Y. Guan, Y. Feng, J. Wan, X. Yang, L. Fang, X. Gu, R. Liu, Z. Huang, J. Li, J. Luo, C. Li, Y. Wang, Small 14 (2018) 1800697.
[26] Q. Xiang, J. Yu, J. Mietek, J. Am. Chem. Soc. 134 (2012) 6575–6578.
[27] B. Chen, Y. Meng, J. Sha, C. Zhong, W. Hu, N. Zhao, Nanoscale 10 (2018) 34–68.
[28] G. Liu, A.W. Robertson, M.J. Li, W.C.H. Kuo, M.T. Darby, M.H. Muhieddine, Y.C. Lin, K. Suenaga, M. Stamatakis, J.H. Warner, Nature Chem. 9 (2017) 810–816.
[29] J. Liang, C. Wang, P. Zhao, Y. Wang, L. Ma, G. Zhu, Y. Hu, Z. Lu, Z. Xu, Y. Ma, ACS Appl. Mater. Interfaces 10 (2018) 6084–6089.
[30] Y. Shi, Y. Zhou, D.R. Yang, W.X. Xu, C. Wang, F.B. Wang, J.J. Xu, X.H. Xia, H.Y. Chen, J. Am. Chem. Soc. 139 (2017) 15479–15485.
[31] H. Liu, K. Tian, J. Ning, Y. Zhong, Z. Zhang, Y. Hu, ACS Catal. 9 (2019) 1211–1219.
[32] Y. Liu, G. Zhu, J. Gao, M. Hojamberdiev, R. Zhu, X. Wei, Q. Guo, L. Peng, Appl. Catal. B-Environ. 200 (2017) 72–82.
[33] Y. Cao, Z. Xing, Z. Li, X. Wu, M. Hu, X. Yan, Q. Zhu, S. Yang, W. Zhou, J. Hazard. Mater. 343 (2017) 181–190.
[34] Y. Qu, Z. Li, W. Chen, Y. Lin, T. Yuan, Z. Yang, C. Zhao, J. Wang, C. Zhao, X. Wang, F. Zhou, Z. Zhuang, Y. Wu, Y. Li, Nature Catal. 1 (2018) 781–786.
[35] F. Wang, Y. Wang, Y. Feng, Y. Zeng, Z. Xie, Q. Zhang, Y. Su, C. Ping, L. Yang, K. Yao, Appl. Catal. B-Environ. 221 (2017) 510–520.
[36] Y. Wang, Z. Xu, C. Di, W. Yan, Y. Zhu, Appl. Catal. B-Environ. 211 (2017) 79–88.
[37] X. Fang, Q. Shang, Y. Wang, L. Jiao, T. Yao, Y. Li, Q. Zhang, Y. Luo, H.L. Jiang, Adv. Mater. 30 (2018) 1705112.
[38] X. Li, W. Bi, L. Zhang, S. Tao, W. Chu, Q. Zhang, Y. Luo, C. Wu, Y. Xie, Adv. Mater. 28 (2016) 2427–2431.
[39] H. Li, L. Wang, Y. Dai, Z. Pu, Z. Lao, Y. Chen, M. Wang, X. Zheng, J. Zhu, W. Zhang, Nature Nanotech. 13 (2018) 411–417.
[40] P. Liu, Y. Zhao, R. Qin, S. Mo, G. Chen, L. Gu, D.M. Chevrier, P. Zhang, Q. Guo, D. Zang, Science 352 (2016) 797–801.
[41] C. De La Cruz, N. Sheppard, Spectrochim. Acta 50A (1994) 271–285.
[42] K. Yong-Tae, O. Kazuyoshi, H. Koichi, U. Tomoya, T. Masaki, S. Hiroyoshi, M. Tadaoki, Angew. Chem. Int. Ed. 45 (2006) 407–411.
[43] Y. Gao, W. Yan, Z. Hui, Appl. Catal. B-Environ. 178 (2015) 29–36.
[44] U. Caudillo-Flores, M.J. Muñoz-Batista, A.B. Hungría, M.L. Haro, M. Fernández-García, A. Kubacka, Appl. Catal. B-Environ. 245 (2019) 49–61.
[45] J. Kong, X. Lai, Z. Rui, H. Ji, S. Ji, Chin. J. Catal. 37 (2016) 869–877.
[46] S. Sun, J. Ding, J. Bao, C. Gao, Q. Zeming, X. Yang, B. He, C. Li, Appl. Surf. Sci. 258 (2012) 5031–5037.
[47] V. Augugliaro, S. Coluccia, V. Loddo, L. Marchese, G. Martra, L. Palmisano, M. Schiavello, Appl. Catal. B-Environ. 20 (1999) 15–27.
[48] J.X. Liang, X. Yang, A.Q. Wang, T. Zhang, J. Li, Catal. Sci. Technol. 6 (2016) 1017–1036.